INSTITUTE OF PHYSICS PUBLISHING MEASUREMENT SCIENCE AND TECHNOLOGY

Meas. Sci. Technol. **17** (2006) 3094–3101 doi:10.1088/0957-0233/17/11/030

Design and characterization of an atomic beam source with narrow angular divergence for alkali-earth targets

Andrew James Murray, Martyn J Hussey and Michael Needham

School of Physics and Astronomy, University of Manchester, Manchester M13 9PL, UK

E-mail: Andrew.Murray@manchester.ac.uk

Received 18 September 2006
Published 19 October 2006
Online at stacks.iop.org/MST/17/3094

Abstract

A new atomic beam source for use in laser-based experiments is described and characterized. The physically collimated source which has been tested using calcium, produces an atomic beam with low angular divergence and narrow transverse Doppler profile, as measured using fluorescence techniques with a near resonant laser beam. The low angular divergence of the source is essential for new experiments which study super-elastic scattering of electrons from laser prepared targets within a magnetic field, since the atomic beam must pass through a narrow gap between the coil windings. The beam density for calcium is calculated to be 2.8×10^9 atoms cm^{-3} when the source is operated at a temperature of 1090 K. This is sufficient to produce good electron energy loss and super-elastic scattering signals, while ensuring negligible radiation trapping within the atomic beam.

Keywords: atomic beam source, atomic oven, super-elastic scattering, laser-atom excitation

(Some figures in this article are in colour only in the electronic version)

1. Introduction

The need for metal-vapour targets in atomic physics experiments is increasing with the advent of new techniques, including atom cooling and trapping [1], the production of Bose–Einstein condensates [2], production of nano-structures using light forces [3] and collision experiments [4–6]. In many experiments there is a requirement to produce a high-density atomic beam which is well collimated, so that the transverse Doppler profile of the beam is minimized and unwanted deposition onto the vacuum chamber surfaces is reduced.

By operating within these criteria, it is possible to effectively manipulate atomic beams using light forces. As an example, optical forces can be used to further collimate the atomic beam using near-resonance laser beams in an optical molasses, which reduces the transverse velocity to near zero [1]. This technique is often used prior to insertion of the atomic beam into a Zeeman slower, where both the longitudinal velocity and phase space density are reduced [1]. A slow atomic beam from the Zeeman slower is then usually captured in a magneto-optical trap where experiments are conducted using these cold atoms [7].

A second important use for well-collimated atomic beams is in collision experiments. In this case, an electron beam (ion beam, or neutral atom/molecule beam) of well-controlled momentum interacts with the target atoms, and the products of the interaction are studied. Processes investigated include elastic scattering, where the incident electron changes momentum without changing energy, inelastic scattering processes where the incident electron loses energy leaving the target in either an excited or ionized state, and super-elastic scattering experiments where the target atom is prepared in an excited state using resonant laser radiation prior to the collision. In the latter case, the electron leaves the interaction region with higher energy than the incident beam, and the target returns to the ground state.

All these experiments benefit from the atomic beam source being well collimated, and having high density. An important further consideration is that collimation of the atomic beam

substantially reduces contamination of the vacuum chamber, which can have severe detrimental effects on the experiment that is being performed [8]. In particular, atoms from the source may react with components inside the vacuum chamber so as to damage sensitive and expensive parts. It is therefore essential to reduce contamination to a minimum.

A further advantage arises during experiments which use narrow-band laser excitation. In these experiments, a resonant laser beam excites the atoms prior to measurement. The efficiency of excitation, and hence density of excited targets, depends on the relative frequency of the laser beam with respect to the atomic transition frequency. The laser frequency as seen by the atoms depends on their velocity component in the direction of the laser beam, giving rise to the Doppler shift. For transverse excitation, where the laser beam is directed orthogonal to the atomic beam, this shift is minimized by ensuring the target beam is well collimated, producing a greater proportion of atoms in the excited state.

It is also essential to collimate the target beam for new super-elastic scattering experiments being performed at Manchester. In these experiments, a Magnetic Angle Changing (MAC) device [9, 10] steers electrons into and out of the interaction region using a well-controlled magnetic field. The MAC coils are separated by a distance of 7 mm so that the magnetic field at the entrance to the electron detector and exit from the electron gun are zero. Hence the atomic beam profile must be much smaller than this gap so as to eliminate deposition on the surface of the coils. This is essential for low energy electron scattering experiments, since surface deposits may become charged by stray electrons, producing uncontrolled patch electrostatic fields that seriously disrupt the measurements.

Previous studies using alkali and alkali-earth metals as a target include super-elastic scattering and (e, 2e) ionization measurements at Manchester [8, 11], where the atoms were produced from an effusive source [12]. This source [12] produced a high density of atoms, but suffered from extremely poor collimation (∼30° angular spread) and so severely contaminated the spectrometer, damaging components during operation. As such, it could not be used in the present super-elastic scattering experiments. Other studies using calcium as a target include electron impact experiments [13–18], early super-elastic scattering experiments [19], photo-ionization studies using synchrotron radiation and pulsed laser photo-ionization studies [20–25]. Ross and Sontag [26] extensively review different atomic beam sources, and so provide an invaluable resource for their design.

In this paper a new source is detailed. The source has been characterized using calcium; however, it is expected to deliver similar performance with other alkali-earth targets as the required operating temperature is highest for calcium. The severe deficits of the previous design detailed in [8, 12] have been eliminated, so that the beam is now well collimated using physical apertures and skimmers, and so does not contaminate the interior of the chamber. The new oven operates with a single heater element in contrast to the previous design, making this substantially cheaper to build, and is mounted on an adjustable table for accurate alignment to the interaction region. As such it is a significant advance on the previous source. Full CAD drawings of the oven and its mount are available by contacting the authors. The constant current supply which drives the heater element is also described here, allowing a complete system to be constructed. CAD drawings of the PCB layouts are also available.

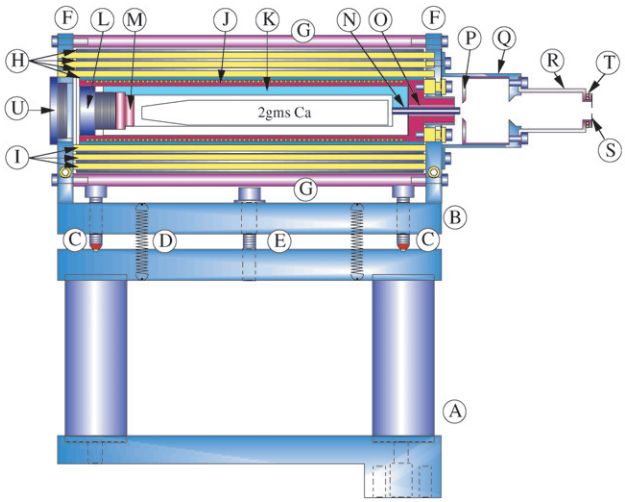

Figure 1. The new atomic beam source, showing a charge of Ca in the crucible. For details, see the text.

2. Design of the atomic beam source

A scaled drawing of the new oven is shown in figure 1. The assembly mounts on an adjustable stand (A) which connects directly to the spectrometer baseplate. The lower mounting plate is 'L' shaped to allow a turntable to pass below the base-plate. Four 20 mm diameter pillars secure the top-plate to the base-plate as shown. The oven mounting yoke (B) is secured to the base-plate (A) via adjusting screws (C) which have a single point contact through ruby balls onto which these screws locate. Four non-magnetic springs (D) constructed from beryllium–copper [27] ensure that the yoke (B) remains in contact with the base-plate via the adjustment screws (C) while the oven is aligned to the interaction region. Upon alignment, locking screws (E) are engaged to ensure the complete mount is secured.

The oven assembly is constructed between two face-plates (F) which are fixed to the yoke (B) using 2 mm diameter A4 grade stainless steel fixing screws. This allows the complete oven assembly to be removed from the mounting plates for maintenance, while ensuring that the position of the oven can be re-established. The face-plates (F) are separated by three stainless steel rods (G) which minimizes thermal contact.

The oven consists of four concentric heat shielding cylinders (H) constructed from 310 grade stainless steel. The heat shields are separated by 2 mm OD thin walled ground ceramic rods (I) accurately spaced apart by locating the rods into guide holes drilled through the face-plates (F). The use of thin walled ceramics ensures minimum thermal contact between the heat shields, while ensuring they are equally spaced apart. The heat shields are 4 mm shorter than the distance between the face-plates (F) to eliminate thermal contact with these plates.

The oven heater (J) is constructed from an oxygen free copper jacket, around which 3.2 m of 1 mm diameter thermo-coax [28] is wound in a spiral configuration. The heater spiral changes pitch at the nozzle end of the copper jacket, so that an increased length of heater can be wound at this end. This ensures that the nozzle is slightly hotter than the body of the oven. The thermo-coax is terminated at the nozzle end of the oven using a ceramic mounted copper junction clamp exterior to the oven assembly.

The oven crucible (K) is constructed from 310 grade stainless steel with an internal diameter and length that allows a 1–2 gram ampoule of high purity material to be installed. This new design allows the ampoule to be inserted into the oven after the neck has been broken off, the filling being carried out under argon. The crucible is then closed using the screw (L) which pushes the seal (M) onto the internal knife edge of the crucible (not shown).

The seal (M) is constructed from 310 grade stainless steel rather than copper, as is usually used for alkali metals. This is found to be necessary from previous experience [8], since alkali-earth targets such as calcium react vigorously with copper when hot, rapidly destroying the seal. Alkali-earth targets sublime directly to the vapour phase and so remain solid inside the crucible during operation, and the metal to metal seal has been found to be effective in ensuring that the oven does not leak during operation.

The output from the crucible is delivered through a 2 mm OD molybdenum nozzle (N) which is press fitted into the crucible (K). An oxygen free copper cylinder (O) is inserted between the heater orifice and the nozzle to ensure good thermal contact to the nozzle. This technique allows nozzles of different diameters to be used, by re-machining the heat coupling cylinder (O) to fit.

Physical collimation of the oven is achieved using the assembly (P) to (S). A heat shield (P) is fitted inside the skimmer assembly (Q) so that radiation from the heater (J) to the collimator is reduced. The assembly (Q) has a 6 mm diameter skimmer at its exit to reduce the flux of atoms that enter the collimation chamber (R). A constantan aperture (S) is fitted centrally onto the collimation chamber (R) as shown. This aperture is constructed from 0.1 mm thick sheet, and is spot-welded to the front face of the chamber. A heater (T) consisting of two loops of thermo-coax can be wound onto the chamber exit so as to keep the aperture (S) at an elevated temperature (this was not found to be necessary using calcium as the target).

The crucible (K) can be removed from the oven assembly by undoing the screw-bolt (U) from the back face-plate, then withdrawing the crucible from the heater. This ensures that the assembly remains aligned to the interaction region should refilling be necessary.

The collimation factor of the beam source is dictated by the internal diameter of the nozzle (N), the diameter of the output aperture (S) and the distance between the exit of the nozzle and the aperture (S), as long as the region between the nozzle and aperture does not fill with vapour from the target gas. Tests on this source over several months have shown that the collimation/skimmer assembly acts as an effective beam dump for unwanted vapour, ensuring that the collimation factor is as expected under these conditions.

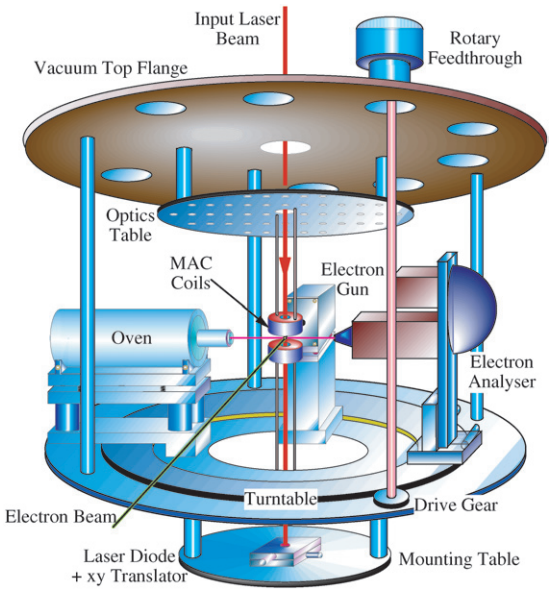

Figure 2. The new vacuum chamber showing the position of the new beam source with respect to the electron gun, electron analyser and MAC coils for use in super-elastic scattering studies. A cold trap opposite the oven is not shown, and a 50 mm diameter $f2$ lens which collects light from the interaction region between the MAC coils is also not shown.

Alignment of the source to the interaction region is facilitated by replacing the crucible with an assembly of equivalent diameter in which a visible laser diode is secured. The laser diode assembly has an output aperture of 1 mm so that the laser beam can be accurately directed through the collimation aperture (S). The oven alignment is then carried out by adjusting the alignment screws (C) so that the laser beam emanating from the oven passes through the interaction region for the experiment. The laser assembly is then removed and the crucible replaced.

3. Constant current drive electronics for the heater supply

It has been found previously [8] that atomic beam sources of this kind can be effectively maintained at a constant temperature within the vacuum chamber by employing a constant current supply, rather than using more complex feedback temperature control systems. This considerably reduces the cost of construction. Temperature monitoring is achieved using two type 'K' thermocouples [28] wound onto the ends of the heater spiral of the copper heater jacket (J), and are brought away from the oven to terminate in shielded LEMO plugs for ease of use.

All connections to the oven are through electrical feed-throughs located on the top flange of the vacuum chamber, to which all internal parts of the spectrometer are secured, as shown in figure 2. In this figure, the spectrometer is shown with the oven source installed onto the base-plate. An electron gun is also secured to this plate, whereas an electron analyser rotates on a turntable around the interaction region. The figure shows the location of the MAC coils through which the atomic and electron beams must pass. A laser

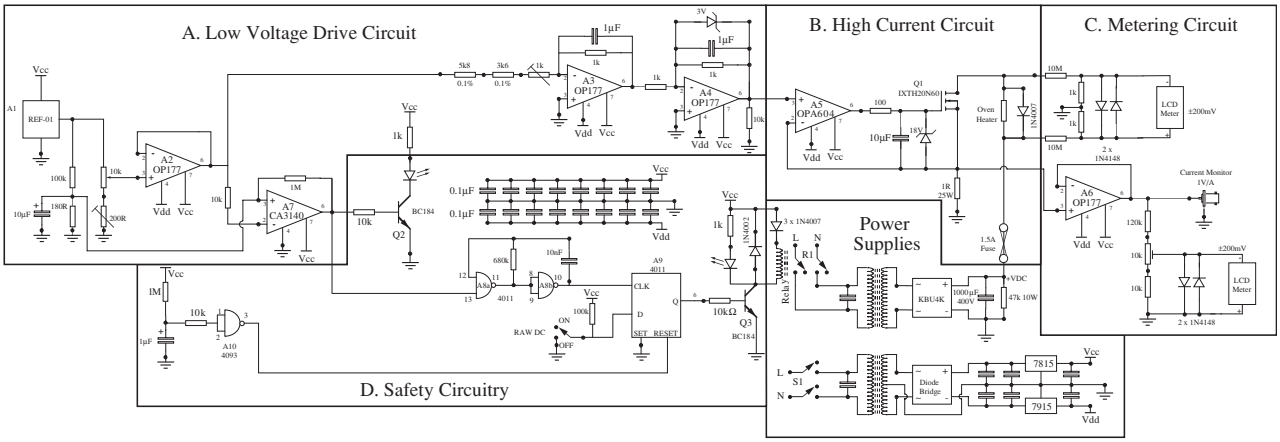

Figure 3. The 1 A constant current supply which has a compliance voltage of 325 V_{dc}. For details, see the text.

beam is also shown passing through the interaction region so as to perform fluorescence measurements (section 4), and to allow super-elastic scattering studies. A 650 nm diode laser located underneath the base-plate is used to align the input laser beam onto the interaction region by providing a tracer beam through the input window. A stainless steel liquid nitrogen cooled cold trap [29] (not shown) is placed opposite the oven so as to collect vapour which has passed through the interaction region. A 50 mm diameter $f2$ lens (not shown) collects fluorescence from the interaction region. This lens images the interaction region through a vacuum window onto a photodiode located outside the chamber, so as to measure fluorescence and Doppler profiles of the atomic beam.

The constant current supply that feeds the heater for the oven uses a high power MOSFET to pass controlled current through the heater load, as shown in figure 3. The dc supply to the MOSFET is set to ensure sufficient current can be delivered to the load, while maintaining the transistor within a linear operating regime. In practice, the crucible is heated to ∼1100 K using a current of 0.45 A. The total length of thermo-coax wound onto the copper heater jacket is 3180 mm, which has a resistance of 275 Ω when hot (270 Ω when cold). The potential across the heater is therefore 120 V for a power delivery of 53 W.

The supply uses a simple pass controller (B) to establish constant current into the load. MOSFET Q1 acts as the pass transistor and is secured onto a fan-cooled heat-sink to ensure thermal dissipation during operation. The oven heater load connects via a 1.5 A fast-blow fuse directly between the dc supply and the drain of Q1. A 1 Ω 25 W resistor between the source of Q1 and 0 V (earth) provides negative feedback to amplifier A5, so as to ensure the current passing through the drain (and hence the source) is held constant. The current is adjusted by applying a control voltage to the input of A5 using the low voltage control circuitry (A), so that 1 V_{dc} on the input passes 1 A through the heater. The additional circuitry around Q1 ensures protection of the device should failure of the power supply or load occur. Two front panel mounted liquid crystal meters provide information on the current and voltage supplied to the heater, as shown in circuitry (C) of the figure.

Safeguards are provided by circuitry (D) in the figure, which ensures that the high voltage supply cannot be turned on or off unless the output voltage has been set near zero, at which time relay R1 can be switched. R1 engages the mains supply to the transformer which provides the unregulated dc supply to the load. The low voltage ±15 V_{dc} supplies are provided by standard circuitry, and are engaged upon switching the front panel mains switch S1 on.

The output of the constant current supply is connected via a 3-terminal high voltage LEMO connector using shielded twin-core cable to deliver current via the spectrometer feed-through. All connections within the spectrometer are also fully shielded and use PTFE coated wire. Full details of the supply can be obtained from the authors.

4. Characterization of the atomic beam

The source presented here is required to deliver high flux with narrow angular spread, while ensuring radiation trapping is minimized. To measure the atomic beam characteristics, a near resonant laser beam at ∼423 nm is directed through the interaction region (figure 2). Fluorescence is then monitored using a 50 mm diameter lens located 175 mm from the interaction region, which images the fluorescence onto an amplified photo-diode located external to the vacuum chamber. The fluorescence is collected orthogonal to both the atomic beam and laser beam, so that the Doppler profile and fluorescence characteristics of the ensemble can be determined.

Several characteristics of the atomic beam can be established. By changing the temperature of the oven, the intensity of emitted radiation can be monitored to establish the relative change in density of the beam. The effects of radiation trapping of light within the beam can also be established by monitoring the polarization characteristics of this light. The angular spread of the atomic beam is easily viewed using these techniques, and the frequency line width of the atomic beam estimated by scanning the laser wavelength through resonance. This process allows any residual background gas from the oven to be monitored, which shows up as fluorescence not related to the main atomic beam as the wavelength is changed.

By measuring these parameters, the absolute density of atoms emitted from the source can be determined. This requires the excited state population due to laser excitation

to be known, which is estimated using an existing quantum electro-dynamic (QED) model [11]. The model includes effects due to the input laser intensity, the lifetime of the state, the polarization of the radiation and the detuning of the beam.

4.1. Collimation of the atomic beam

The collimation of the atomic beam was established using two methods. Firstly, an image of the interaction region produced by the 50 mm diameter lens was measured, and the magnification of the lens used to determine the size of the atomic beam illuminated by the laser beam. These images indicated that the atomic beam was ∼2 mm in diameter at the interaction region.

A more direct measurement was possible after the oven had been operating for several days. In this case, calcium deposited onto the cold trap located a distance of 220 mm from the interaction region produced a clearly defined spot of diameter 9–10 mm. Since the molybdenum output nozzle of the source had an internal diameter of 1.4 mm and the collimating aperture was 1 mm, the angular divergence of the beam was then estimated as $\pm 1.3^{\circ}$, producing a beam of diameter 2.1 mm at the interaction region. This is consistent with the fluorescence imaging measurements, confirming that the source produced a highly collimated atomic beam as required.

4.2. Fluorescence studies as a function of temperature

For illumination of the atoms by a resonant laser beam of constant intensity, the fluorescence viewed by the collecting lens provides a direct measure of the density of atoms in the interaction region. This relationship holds only if radiation trapping within the atomic beam is insignificant, and so it is necessary to measure the polarization of the emitted fluorescence to ascertain these effects. Details of radiation trapping measurements are given below.

Fluorescence measurements were carried out by heating the oven to 1100 K, and then letting the oven slowly cool by gradually reducing the heater current. From these studies the fluorescence intensity (which is directly proportional to the beam density) was found to increase exponentially with temperature, the increase being an order of magnitude for each 127 K increase in temperature. This type of density variation is typical for this type of effusive source [26]. The oven temperature was maintained below 1100 K to ensure that the calcium remained in a solid form throughout the measurements.

4.3. Measurement of radiation trapping in the beam

The density of the atomic beam can critically effect many experiments such as super-elastic scattering studies from laser excited atoms, if it is sufficiently high to trap radiation within the beam. This *radiation trapping* process [30, 31] is particularly severe if the transition excited by the laser involves the ground state. Radiation trapping effectively *increases* the measured lifetime of the state, and depolarizes the observed radiation. This process occurs when atoms in the ground state capture a photon emitted from a nearby excited atom undergoing relaxation, before the photon can escape the interaction region. As the density of ground-state atoms increases, the probability of re-absorption and delay in emission from the interaction region also increases. The polarization of emitted fluorescence *decreases* with radiation trapping, since the trapping atoms may re-emit the absorbed photon in a different direction, with a different polarization state. In the limits of severe radiation trapping, the measured lifetime of the state increases to many times the natural lifetime, and the degree of polarization of the scattered radiation reduces to zero.

Super-elastic scattering measurements are particularly sensitive to radiation trapping, as the parameters which are measured depend critically on the polarization of the light exciting the transition. As such, it is essential to ensure that these effects are minimized, while producing a beam density high enough for the experiments to be viable.

To establish the effects of radiation trapping from this source, a linearly polarized laser beam was directed through the interaction region with the laser polarization vector pointing along the atomic beam direction, so as to maximize fluorescence collected by the lens. The polarization of the emitted light was then determined by rotating an analysing polarizer (extinction ratio $1{:}10^5$) through multiples of 2π. These measurements were conducted at a temperature of 1090 K, resulting in a degree of polarization $P_1 = 99.8\% \pm 0.04\%$. At this and lower oven temperatures the effects of radiation trapping can therefore be neglected. This is principally due to the high collimation factor of the beam, resulting in very low background vapour outside the target beam in the direction of the collecting lens.

4.4. Measurement of the line-width

An important factor for laser interaction studies is the line-width of fluorescence from the atomic beam. This line-width is given by three factors: the natural line-width given by the spontaneous emission rate, the line-width due to resonant laser radiation interactions (power broadening), and the Doppler width which is given by the physical properties of the atomic beam. The natural line-width for the $4^1\,\mathrm{P}_1 \xrightarrow{423\,\mathrm{nm}} 4^1\,\mathrm{S}_0$ decay transition in calcium is 34.6 MHz, resulting from a spontaneous decay rate of 4.6 ns. The Doppler width is determined from the divergence of the atomic beam, and the velocity component perpendicular to the laser beam of the beam flux. Power broadening due to the laser intensity depends on the Rabi frequency, which determines the absorption and stimulated emission rates under the influence of laser radiation.

For a simple atomic system such as calcium, it is possible to model the laser interaction accurately using rate equations. This model has been detailed in [11], where it is shown that the normalized steady state population of the upper excited state may be written as follows:

$$\rho_{22} = \frac{4\eta^2 I_{\mathrm{Las}}}{8\eta^2 I_{\mathrm{Las}} + \Gamma_2^2 + 4\delta^2}. \tag{1}$$

Here I_{Las} is the intensity of the laser beam measured in mW mm^{-2}, $\Gamma_2 = 2.174 \times 10^8$ rad s^{-1} is the natural decay rate, $\eta = 9.95 \times 10^7$ is a constant (see [11]) and δ is the detuning from resonance of the radiation as seen by the atoms.

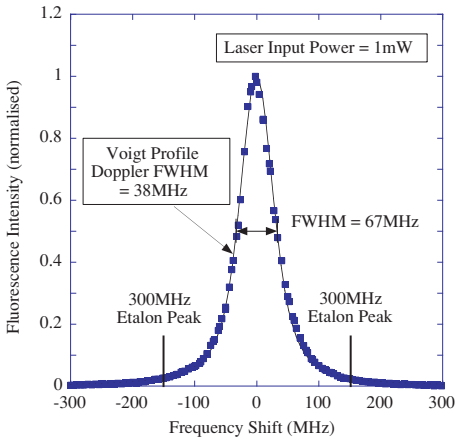

Figure 4. Measurement of the line profile of the fluorescence from the atomic beam as a function of laser frequency from resonance, normalized to unity on resonance. The input laser power was 1 mW for these studies, and a Voigt profile has been fitted to the data to ascertain a Doppler width of 38 MHz. For details, see the text.

For laser radiation of fixed polarization and direction, the intensity of fluorescence collected by the lens is directly proportional to ρ_{22}, and can be measured as a function of laser frequency. Equation (1) describes the excited state population without Doppler detuning, and yields a Lorentzian line-shape which broadens with increasing laser intensity. The effects of the Doppler profile can be incorporated by integrating the resulting fluorescence signal over the geometry of the atomic and laser beams. This yields a line-shape described by a Voigt profile $V(\delta)$, produced from the convolution of the Doppler profile with a Lorentzian:

$$V(\delta) = \frac{1}{\sigma_D\sqrt{\pi}} \int_{-\infty}^{+\infty} \rho_{22}(\delta - \omega) \exp\left(-\frac{\omega^2}{\sigma_D^2}\right) \mathrm{d}\omega \qquad (2)$$

where σ_D is the line-width associated with the Doppler profile. The Voigt profile does not have a simple analytic form, and so must be fitted numerically to experimental data.

To ascertain the line-width of the fluorescence, the laser beam intensity was reduced to $\sim$280 μW mm^{-2} (laser power 1 mW into the vacuum chamber) and the fluorescence collected by the 50 mm diameter lens was measured as a function of laser detuning. The laser frequency shift was monitored using a 300 MHz Fabry–Perot interferometer, so as to accurately determine the relative frequency of the laser beam.

Figure 4 shows the result of these studies as a function of detuning from resonance. Voigt profiles with different σ_D were generated from equation (3), and the variances between the experimental data and different profiles were compared. The variance was found to be a minimum for a profile which had a Doppler profile with $\sigma_D = 38$ MHz. The FWHM for the Voigt profile was then 67 MHz.

The Doppler width evaluated from the Voigt profile agrees well with that estimated from the geometry of the atomic beam produced from the oven, where it is found that the angular divergence of the atomic beam is $\pm 1.3^\circ$. The Doppler shift estimated from the Maxwell–Boltzmann distribution is then given by $\delta_D = \pm 20$ MHz, in close agreement with the 38 MHz FWHM derived above.

In practice the experiment is operated with an input laser power of 70 mW–100 mW, rather than the 1 mW used in the above experiments, so as to maximize the upper state population. In this case power broadening dominates the interaction, and the FWHM of the Voigt profile is found to broaden to 250 MHz. This is as expected from the dominance of power broadening compared to the Doppler profile and natural line-width.

4.5. Measurement of the beam density as estimated from the fluorescence

The experimental data presented above show that the model for the laser atom interaction provides an accurate assessment of the excited state population. Tests of radiation trapping in the beam indicate that this effect is also negligible, and so it becomes possible to estimate the atomic beam density in the interaction region directly from the fluorescence collected by the lens which is imaged onto the photodiode.

To carry out these measurements it is necessary to establish the fraction of total fluorescence collected by the lens to determine the relative population of excited atoms throughout the interaction region, and to calibrate the photodiode. The fraction of light collected by the lens can be determined from the fluorescence radiation profile, which depends on the direction of the laser polarization vector exciting the ensemble. Since radiation trapping is negligible, light emerging from atoms excited with linearly polarized radiation is emitted as a dipole radiation pattern. In these experiments, the input laser polarization vector was set linear, and was rotated to maximize the fluorescence collected by the lens.

To calculate the power radiated by the atoms which is collected by the lens and transmitted to the photodiode, it is necessary to numerically integrate the intensity from the radiating Dipole over the area of the lens situated a distance $d = 175$ mm from the interaction region. Allowing for reflection losses at the lens and window, the total power measured by the photodiode/amplifier outside the vacuum chamber was calculated to be $P_{\mathrm{PD}} = 0.013 P_{\mathrm{tot}}$.

The photodiode was calibrated using an attenuated laser beam operating at 422.6856 nm, by comparing the signal to that from a calibrated power meter. At a temperature of 1090 K, the radiated power delivered to the photodiode was found to be $P_{\mathrm{PD}} = 9.6$ μW, and so the total power emitted by the excited ensemble in the interaction region was $P_{\mathrm{tot}} = 740$ μW.

The final step in estimating the atomic beam density was to establish the average excited state population in the interaction region. It is assumed that the density of atoms in the atomic beam is uniform, and that the laser beam has a Gaussian intensity profile (TEM$_{00}$ mode) with a total input power at the interaction region of P_{in} mW, and has a diameter R $\sim$ 1 mm at the interaction region. The intensity of the laser beam is then given by

$$I_{\mathrm{Las}}(r) = 1.30 P_{\mathrm{in}} \exp\left(-\frac{r^2}{r_0^2}\right) \ \mathrm{mW\ mm^{-2}} \qquad (3)$$

Figure 5 shows the geometry of the interaction region considered cylindrical as defined by the laser beam, and which has a height $L = 2$ mm defined by the atomic beam. The profile of the atomic beam is set by the oven apertures located a distance $D = 45$ mm from the interaction region, yielding a

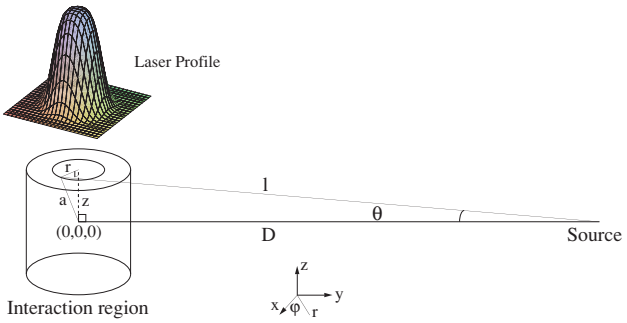

Figure 5. The interaction region defined by the input laser beam (assumed cylindrical) that has a Gaussian TEM_{00} intensity profile. The atomic beam emanating from the source a distance D from the centre of the interaction region has an angular extent of $\theta_{\max} = \pm 1.3^{\circ}$. The cylindrical geometry used for integration is shown.

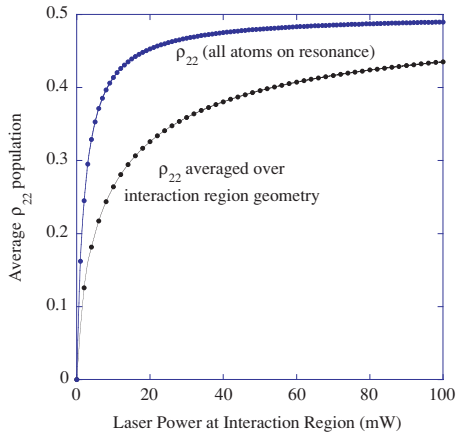

Figure 6. The calculated normalized average excited state population ρ_{22} as a function of laser power at the interaction region. The result is compared to that when all atoms in the interaction region are in resonance with the laser beam. The averaged population rises more slowly with incident laser power and reaches a smaller final value at 100 mW input power. For details of the calculation, see the text.

maximum angular spread of the atomic beam of $\pm 1.3^{\circ}$. The origin (0,0,0) is set at the centre of the interaction region.

By considering the Doppler detuning due to different atomic velocities in the interaction region, it may be shown that the upper state population $\rho_{22}(r, \varphi, z)$ is given by

$$\rho_{22}(r,\varphi,z) = \frac{5.20\eta^2 P_{\text{in}} \exp\left(-\frac{r^2}{r_0^2}\right)}{10.4\eta^2 P_{\text{in}} \exp\left(-\frac{r^2}{r_0^2}\right) + \Gamma_2^2 + \frac{16\pi^2\langle v\rangle^2 z^2}{\lambda^2(r^2+D^2+z^2-2rD\sin\varphi)}}. \quad (4)$$

The average population of excited states which emit radiation is then calculated by numerically integrating $\rho_{22}(r, \varphi, z)$ over the volume of the interaction region.

The result of this analysis as a function of incident laser power is shown in figure 6, compared to the result when all atoms are in resonance with the laser beam. The population of excited atoms is significantly less than when all atoms are on resonance, and rises more slowly as a function of laser power. At an incident power of 75 mW as used in these

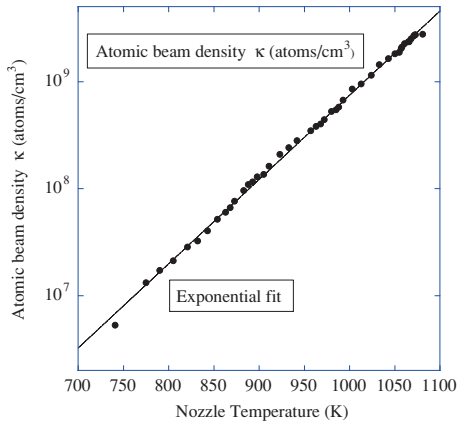

Figure 7. Estimated beam density in the interaction region calculated from fluorescence measurements, showing the exponential increase in density as a function of temperature.

experiments, the average population in the excited state is found to be $\rho_{22}^{\text{Av}}(75\text{ mW}) = 0.42$.

Since the rate of excitation must equal the rate of emission in the steady state, the total rate of photon emission from the interaction region is then given by

$$\Gamma_{\gamma}^{\text{Tot}} = \rho_{22}^{\text{Av}}\Gamma_2\beta \quad (5)$$

where β is the number of atoms in the interaction region. The total power emitted by the atoms P_{tot} is related to the total rate of photon emission $\Gamma_{\gamma}^{\text{Tot}}$ through the photon energy:

$$\Gamma_{\gamma}^{\text{Tot}} = \frac{P_{\text{tot}}}{h\nu} = \frac{\lambda P_{\text{tot}}}{hc} = 1.6 \times 10^{15}\text{ photons s}^{-1}. \quad (6)$$

Hence the total number of atoms in the interaction region β is given by

$$\beta = \frac{\Gamma_{\gamma}^{\text{Tot}}}{\rho_{22}^{Av}\Gamma_2} = \frac{1.6 \times 10^{15}}{0.42 \times 2.174 \times 10^8} = 1.75 \times 10^7\text{ atoms}. \quad (7)$$

Since the density of atoms in the interaction region κ is assumed uniform, the density is then given by

$$\kappa = 2.8 \times 10^9\text{ atoms cm}^{-3}. \quad (8)$$

This density is not untypical for ovens used in photon measurements as indicated in [26], where it is noted that $\kappa < 10^{10}\text{atomscm}^{-3}$ to avoid significant radiation trapping.

Finally, the flux of atoms Φ in the atomic beam can be calculated, and is given by

$$\Phi = \frac{\langle v\rangle\beta}{2R}\text{ atoms s}^{-1} = 6.6 \times 10^{12}\text{ atoms s}^{-1}. \quad (9)$$

The fluorescence results can therefore be related directly to the beam density measured on an absolute scale as shown in figure 7, where κ is plotted on a logarithmic scale, showing the exponential increase as a function of oven temperature.

5. Conclusions and summary

A new highly collimated atomic beam source for alkali-earth targets has been described which uses passive collimation provided by a skimmer and defining apertures. The source efficiently produces an atomic beam of calcium with a density

up to 10^{10} atoms cm^{-3}, and which has negligible radiation trapping in the beam. The Doppler line-width of the beam is only around 40 MHz, which compares with the natural line-width from calcium of 34 MHz. The source is presently being used for super-elastic scattering studies in a magnetic angle changing spectrometer, but would be equally useful in atom trapping and slowing experiments, due to its well-defined beam characteristics. The beam deposits onto a liquid nitrogen cooled cold trap inside the spectrometer, and shows no evidence of contaminating the spectrometer as has plagued previous ovens used in Manchester.

The excellent characteristics of this source has allowed the density of atoms to be calculated in the interaction region from fluorescence studies when the atoms are subjected to a near resonant laser beam. This is an important advancement on previous designs, as it provides a significant step forward in the determination of absolute cross sections in ionization studies. Although not yet tested with other alkali and alkali-earth targets, it is expected that the design will operate effectively since all these targets require lower oven temperatures than calcium.

The heater design for this oven uses a simple single coil thermo-coax heater which is inexpensive, and which can be terminated by the user. The high voltage constant current supply for this heater has been documented here.

To help others build this source or modify it to their needs, a compete set of CAD drawings are available from the authors for both the constant current circuitry and the oven.

Acknowledgments

We would like to thank the Engineering and Physical Sciences Research Council in the UK for supplying funds for this project, and for supplying a postdoctoral research fellowship for one of us (MH). The mechanical and electronic workshops in the Schuster laboratory at the University of Manchester are gratefully acknowledged for their expertise in building the components of this source.

References

[1] Metcalf H J and Van Der Straten P 1999 *Laser Cooling and Trapping* (New York: Springer)
[2] Lu B and van Wijngaarden W A 2004 *Can. J. Phys.* **82** 81
[3] Meschede D and Metcalf H J 2003 *J. Phys. D: Appl. Phys.* **36** R17
[4] Hertel I V and Stoll W 1977 *Adv. At. Mol. Phys.* **13** 113
[5] Li Y and Zetner P W 1994 *Phys. Rev.* A **49** 950
[6] Hall B V, Shen Y, Murray A J, Standage M C, MacGillivray W R and Bray I 2004 *J. Phys. B: At. Mol. Opt. Phys.* **37** 1113
[7] Raab E, Prentiss M, Cable A, Chi S and Pritchard D 1987 *Phys. Rev. Lett.* **59** 2631
[8] Murray A J and Cvejanovic D 2003 *J. Phys. B: At. Mol. Opt. Phys.* **36** 4875
[9] Read F H and Channing J M 1996 *Rev. Sci. Instrum.* **67** 2372
[10] Murray A J, Hussey M, MacGillivray W R and King G 2006 *Ionization, Correlation and Polarization in Atomic Physics, AIP Conf. Proc.* **811** p 179
[11] Murray A J and Cvejanovic D 2003 *J. Phys. B: At. Mol. Opt. Phys.* **36** 4889
[12] Cvejanovic D and Murray A J 2002 *Meas. Sci. Technol.* **13** 1482
[13] Schmitz W, Breuckmann B and Mehlhorn W 1976 *J. Phys. B: At. Mol. Phys.* **9** L493
[14] Pejcev V, Ottley T W, Rassi D and Ross K J 1978 *J. Phys. B: At. Mol. Phys.* **11** 531
[15] Feuerstein B, Zatsarinny O I and Mehlhorn W 2000 *J. Phys. B: At. Mol. Opt. Phys.* **33** 1237
[16] Weber W, Breuckmann B, Huster R, Menzel W, Mehlhorn W, Chen M H and Dyall K G 1988 *J. Electron Spectrosc. Relat. Phenom.* **47** 105
[17] Chen M H, Weber W and Mehlhorn W 1989 *J. Electron Spectrosc. Relat. Phennom.* **49** 77
[18] Cvejanovic D and Murray A J 2003 *J. Phys. B: At. Mol. Opt. Phys.* **36** 3591
[19] Teubner P J O, Karaganov V, Law M R and Farrell P M 1996 *Can. J. Phys.* **74** 984
[20] Bizau J M, Gerard P, Wuilleumier F J and Wendin G 1987 *Phys. Rev.* A **36** 1220
[21] Sato Y, Hayaishi T, Itikawa Y, Itoh Y, Murakami J, Nagata T, Sasaki T, Sonntag B, Yagashita A and Yoshino M 1985 *J. Phys. B: At. Mol. Phys.* **18** 225
[22] Ueda K, West J B, Ross K J, Hamdy H, Beyer H J and Kleinpoppen H 1993 *Phys. Rev.* A **48** R863
[23] West J B, Ueda K, Kabachnik N M, Ross K J, Beyer H J and Kleinpoppen H 1996 *Phys. Rev.* A **53** R9
[24] Ueda K, West J B, Ross K J, Kabachnik N M, Beyer H J, Hamdy H and Kleinpoppen H 1997 *J. Phys. B: At. Mol. Opt. Phys.* B **30** 2093
[25] Beyer H J, West J B, Ross K J and De Fanis A 2000 *J. Phys. B: At. Mol. Opt. Phys.* **33** L767
[26] Ross K J and Sontag B 1995 *Rev. Sci. Instrum.* **66** 4409
[27] Murray A J, Hussey M and Venables A 2005 *Meas. Sci. Technol.* **16** N19
[28] *Thermo-coax* France. http://www.thermocoax.com
[29] Murray A J 2002 *Meas. Sci. Technol.* **13** N12
[30] D'Yakonov M I and Perel V I 1965 *Sov. Phys.—JETP* **20** 997
[31] Masters A T, Murray A J, Pascual R and Standage M C 1996 *Phys. Rev.* A **53** 3884